ADVANCED ELECTRONIC MATERIALS
www.advelectronicmat.de

Electroluminescence from Organometallic Lead Halide Perovskite-Conjugated Polymer Diodes

*Aditya Sadhanala, Abhishek Kumar, Sandeep Pathak, Akshay Rao, Ullrich Steiner, Neil C. Greenham, Henry J. Snaith, and Richard H. Friend**

Organometallic lead perovskite-based solar cells now show power conversion efficiencies of above 20%,[1–6] and function as light-emitting diodes under forward bias.[7,8] We have fabricated diodes with adjacent perovskite and conjugated polymer layers, using orthogonal solvents to spin-coat the polymer on top of the perovskite layer. In forward bias, these devices can demonstrate simultaneous emission from both the luminescent conjugated polymer and perovskite. This provides direct information on electron and hole injection and recombination as a function of device architecture and bias voltage. It also offers a means to produce broadband light emission. These organic–inorganic perovskites have shorter alkyl chain which can fit inside the octahedral crystal unit to form 3D structure and shows luminescence due to free carrier electron–hole recombination.[9] Photoluminescence quantum efficiency (PLQE) up to 70%,[9] has been reported and this makes them a promising candidate for LEDs and lasers.[7,9] These luminescent properties are very different to the previously investigated 2D organic–inorganic perovskites.[10–12]

The high PLQE[9] of perovskite thin films indicates that the recombination is dominated by radiative decay pathways. Radiative emission measured from the active layer and hetero-interfaces in organic photovoltaic diodes (OPVs) has been recently demonstrated as an effective tool to understand the charge dynamic and recombination mechanism.[13] Furthermore, suppressing the recombination by efficient extraction of photogenerated charges enhances the efficiency of PV diodes.[14] Conventional perovskite PV devices use 2,2′,7,7′-tetrakis(*N*,*N*′-di-p-methoxyphenylamine)-9,9′-spirobifluorene (spiro-OMeTAD) as a hole selective contact which is a large band gap nonemissive semiconductor. Replacing it with a light-emitting conjugated polymer as hole transport layer and measuring the EL could reveal the charge recombination dynamics inside the bulk and at the hetero-interface of perovskite PVs, and, therefore the possibility to suppress them.

We use perovskite thin films prepared with both iodide and chloride present in *N*,*N*-dimethylformamide (DMF) solution, ($CH_3NH_3PbI_{3-x}Cl_x$) for which the solid films take up very little chloride.[15,16] Multilayer perovskite-conjugated polymer device were fabricated by using orthogonal solvents to spin-coat the perovskite and the polymer layers. By employing a luminescent conjugated polymer in the polymer-perovskite hybrid devices we can observe simultaneous emission from the hetero-interface of polymer-perovskite on driving the device in forward bias. These devices emit across the spectrum from visible to near-infrared similar to a hybrid LED and the emission spectra of the device was tuned by controlling device architecture and voltage bias. The change in the emission spectra with voltage bias confirms the spatial shift in the recombination zone near the hetero-interface due to change in electric-field. Thus, EL from these hybrid devices can be used as a tool to study the unexplored charge recombination properties near the perovskite-conjugated polymer hetero-interface.

We first looked at diodes with the perovskite layer deposited on a mesoporous scaffold of a metal oxide such as TiO_2 or Al_2O_3 because these are known to provide good PV structures.[17,18] We found excellent PV operation and a high forward current density but very weak EL that decayed within the first few seconds of electrical driving. As we discuss later, we find it necessary to introduce layers to either side of the perovskite that can confine charge carriers within this layer, following well-understood designs developed for organic LEDs.[19,20] We fabricated a range of multilayer structures employing layers of perovskite sandwiched between appropriate electron and hole transporting layers, analogous to the structure of efficient inverted organic photovoltaics (OPV) and OLEDs.[21–24]

One of the important criteria for efficient thin film planar devices is the uniformity of the perovskite film.[1,2,25] Efforts were made to optimize the uniformity of the solution-processed perovskite films used in our devices (Figure S1, Supporting Information). **Figure 1**(a) shows a schematic of PV device structure ITO/TiO_2/Perovskite/Spiro-OMeTAD/MoO_x–10 nm/Au. Figure 1(b) shows the flat-band energy level diagram of the device. Literature reports for energy levels were used,[17,26] where the valence band is measured by ultraviolet photoelectron spectroscopy and the position of the conduction band is estimated from the optical band gap. Figure 1(c) shows the SEM cross-section of this device.

Figure 2(a) shows the absorption spectra of the perovskite thin films, and the conjugated polymer MEH–PPV (Poly[2-methoxy-5-(2′-ethylhexyloxy)-1,4-phenylenevinylene]) measured using photothermal deflection spectroscopy (PDS), which is a sensitive absorption measurement technique.[27–29]

A. Sadhanala, Dr. A. Kumar, Dr. S. Pathak, Dr. A. Rao, Prof. U. Steiner, Prof. N. C. Greenham, Prof. R. H. Friend
Cavendish Laboratory
Department of Physics
University of Cambridge
J. J. Thomson Avenue, Cambridge CB3 0HE, UK
E-mail: rhf10@cam.ac.uk
Dr. S. Pathak, Prof. H. J. Snaith
Clarendon Laboratory
Department of Physics
University of Oxford
Parks Road, Oxford OX1 3PU, UK

DOI: 10.1002/aelm.201500008

ADVANCED ELECTRONIC MATERIALS
www.advelectronicmat.de

www.MaterialsViews.com

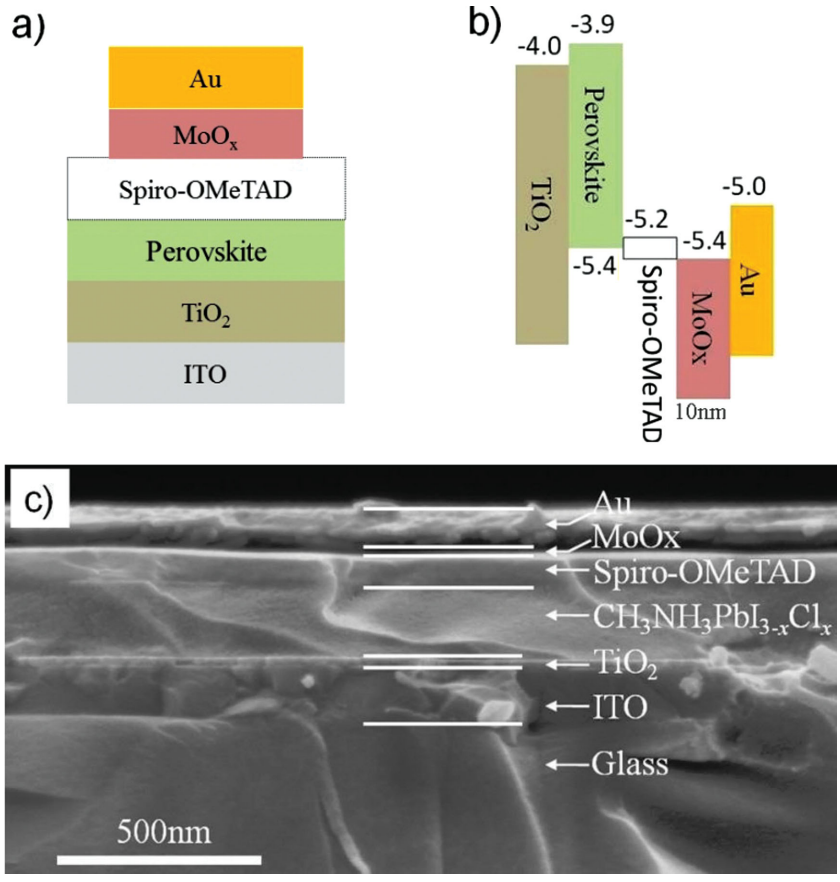

Figure 1. a) Schematic showing the device structure where a 350 nm layer of perovskite was sandwiched between a TiO_2 compact layer acting as electron-transport layer (ETL) and spiro-OMeTAD layer acting as hole-transport layer (HTL) combined with 10 nm MoO_x acting as hole-injection layer and b) the flat band energy level diagram of the device. c) Scanning electron micrograph (SEM) showing the cross section of the ITO/TiO_2/Perovskite/Spiro-OMeTAD/MoO_x–10 nm/Au device with a 350 nm perovskite film.

In Figure 2(a), the perovskite absorption spectra shows a sharp band edge and a clean band gap in contrast to MEH–PPV which has a rather shallow band-edge with presence of trap states within the sub bandgap energy levels. The inset in Figure 2(a) compares the extracted Urbach energies "E_u" (a measure of energetic disorder) for the perovskite and MEH–PPV and shows that the perovskite film has remarkably low energetic disorder with an Urbach energy of ≈13 meV compared to 6.7 meV for GaAs,[28] and 34 meV for MEH–PPV. The surprisingly low Urbach energy of the solution processed perovskite thin film is one of the important reasons behind its efficient performance in PV devices.[27,29]

Figure 2(b) shows the PV characteristic of ITO/TiO_2/Perovskite/Spiro-OMeTAD/MoO_x/Au devices with a 2 nm MoO_x thickness. The devices yielded reasonable power conversion efficiency (η) of 8% and high open-circuit voltage (V_{OC}) of 0.95 V. Figure 2(c) shows the EL spectrum of device driven in forward bias. The emission peak was at 775 nm and the full-width at half-maximum (FWHM) of the emission was ≈41 nm. The EL emission peak was at the same wavelength as the photoluminescence emission peak and was red-shifted from the absorption edge by ≈25 nm. However, when measured in forward bias as a LED, the efficiency of the EL emission from these PV devices was poor (Figure S3, Supporting Information). We consider that the low EL efficiency in these devices is due to the imbalance of the electron and hole current in the device and non-confinement of the charge carriers.

We increased the thickness of the interfacial MoO_x layer from 2 to 10 nm and the EL emission efficiency increased significantly. Figure 2(d) shows the current–density versus voltage (J–V) characteristic of the ITO/TiO_2/Perovskite/Spiro-OMeTAD/MoO_x/Au device with 10 nm thick MoO_x interlayer. The figure also plots the external quantum efficiency (EQE) of electroluminescence emission for this device calculated from the forward emission assuming Lambertian emission over the forward half sphere. The increase in the current after 1 V coincides with the onset of the emission from the perovskite layer, therefore indicating injection of electrons and holes into the perovskite layer, followed by recombination. This device showed broadly stable and reversible characteristics up to current densities of 420 mA cm^{-2} at a bias of 7 V, though there is some dependence on bias voltage history, see Figure S2, Supporting Information. The devices yielded a peak emission EQE of ≈0.024% at 5.8 V bias and 305mA cm^{-2} current density. The MoO_x layer is generally used at a thickness of around 2 nm as a p-doping layer that provides ohmic contacts with many organic semiconductors,[30] and our result shows that higher EL can be obtained by using thicker 10 nm layer. We consider that in this case the thicker MoO_x layer provides a barrier to electron transport and this may help balance electron and hole currents into the perovskite layer. Though the EL efficiency obtained from these PV devices were low compared to the state-of-the art perovskite LEDs,[7] recently demonstrated structural modification of perovskite provides a promising path for future enhancement.[31–33]

The above PV devices have Spiro-OMeTAD as a hole injecting contact which is a large band gap non-emissive semiconductor.[34] To probe the recombination at this hetero-interface we replaced the Spiro-OMeTAD hole selective contact with MEH–PPV, which is a good electroluminescence polymer.[35] By incorporating a luminescent polymer (MEH–PPV) layer as a hole selective contact, we now can expect to see the recombination in the MEH–PPV layer at the perovskite-polymer hetero-interface in the form of electroluminescence when a device is driven in forward bias. We fabricated ITO/MoO_x/perovskite/MEH–PPV/Al multilayer structure with a 6 nm MoO_x thickness as shown in **Figure 3**(a). Under forward bias electrons are injected from the Al cathode and holes are injected from the MoO_x-coated ITO anode and the device yielded simultaneous emission from MEH–PPV at 600 nm and perovskite at 775 nm (Figure 3(a)). The EL efficiency, photon flux intensities and dark

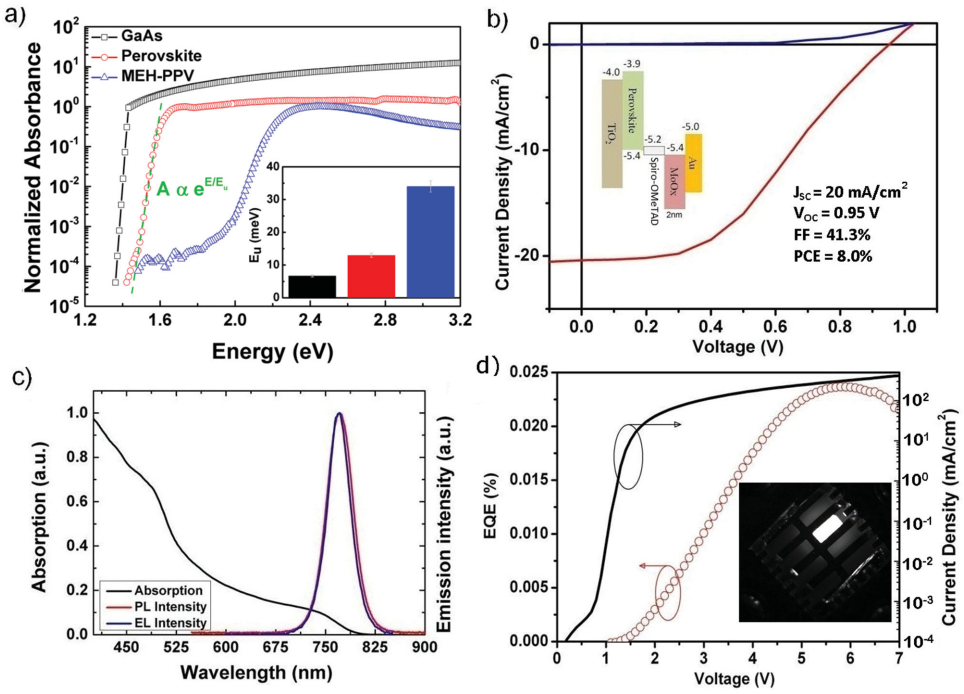

Figure 2. a) Normalized absorbance spectra for GaAs, perovskite ($CH_3NH_3PbI_{3-x}Cl_x$) and polymer MEH–PPV measured using PDS. Inset shows the extracted Urbach energy E_u for these materials along with the fitting error. b) Current density–voltage characteristic of the ITO/TiO_2/Perovskite/Spiro-OMeTAD/MoO_x-2 nm/Au device in the dark and under simulated AM 1.5 G illumination at 100 mW cm^{-2}. c) Typical absorption and photoluminescence spectra for the perovskite layer, and electroluminescence spectrum of the perovskite PV device (ITO/TiO_2/Perovskite/Spiro-OMeTAD/MoO_x–10 nm/Au); d) EQE and current density as a function of voltage for this device operating as an LED under forward bias. Inset shows a photograph of the emission from a device at 6 V bias using an infra-red camera, demonstrating uniform emission. The light emitted from the edge in the photograph is the additional light guided through the glass substrate and perovskite film. The data for GaAs are adapted from Miller et al.[28]

J–V characteristics of these devices are quantified in Figure S5, Supporting Information. When we inverted the injection of electrons and holes by using the device structure ITO/TiO_2/perovskite/MEH–PPV/MoO_x with a 10 nm MoO_x layer is shown in Figure 3(b), we observed emission from the perovskite layer only. Here, the injection of electrons from the conduction band of perovskite to the LUMO of MEH–PPV is energetically unfavorable and therefore the emission from MEH–PPV layer was absent. The PV characteristics of this device are shown in the Figure S6, Supporting Information.

The simultaneous emission from perovskite and MEH–PPV in Figure 3(a) indicates either (i) the transfer of injected electrons from the LUMO of MEH–PPV to the conduction band of perovskite and the transfer of injected holes from the valence band of perovskite to the HOMO of MEH–PPV, or (ii) electron–hole recombination in the MEH–PPV close to the perovskite interface, followed by energy transfer to the perovskite. The spectral overlap of MEH–PPV emission and perovskite absorption (Figure S4, Supporting Information) does indicates the possibility of radiative energy transfer through reabsorption of the EL emission from the MEH–PPV layer into the perovskite layer. However, when we further investigated the emission spectrum of the device with increasing the voltage bias (Figure 3(c)) we found that the ratio of the emissions from the perovskite and the MEH–PPV layer changed with the bias voltage, which indicates that energy transfer by reabsorption plays the smaller role.

Measurement of the PL emission for bilayer structures with excitation and detection from the top and the bottom revealed that around 60% of MEH–PPV emission is reabsorbed in the 350 nm thick perovskite layer used in this work (Figure S4, Supporting Information). Possibly, further optimization the thickness of the perovskite layer (for example, at 35 nm its absorption of emission from MEH–PPV would be only 6%) would suppress the reabsorption but this requires a higher level of control of thickness in each layer in order to maximize the overall emission.

Figure 3(c) shows the electroluminescence spectra of ITO/MoO_x/perovskite/MEH–PPV/Al device with a 10 nm MoO_x layer, at different applied voltages. At 4 V, the device turned on and we observed weak emission from MEH–PPV polymer only. At 5 V the emission from MEH–PPV increased, however we also observed a weak emission at 775 nm, which corresponds to the emission of the perovskite layer. At 6 V bias the emission from MEH–PPV and perovskite both increased and from 7 V onwards the emission from MEH–PPV decreased while the emission from perovskite increased further. The change in the emission spectrum with voltage bias indicates that the electron–hole recombination zone in the device changed spatially with the applied electric field.[36] Zaumseil et al. observed a similar spatial movement of the electron–hole recombination zone from the cathode to the anode by tracked the emission profile of an ambipolar polymer light-emitting-field-effect-transistor by increasing the voltage bias, however such technique is

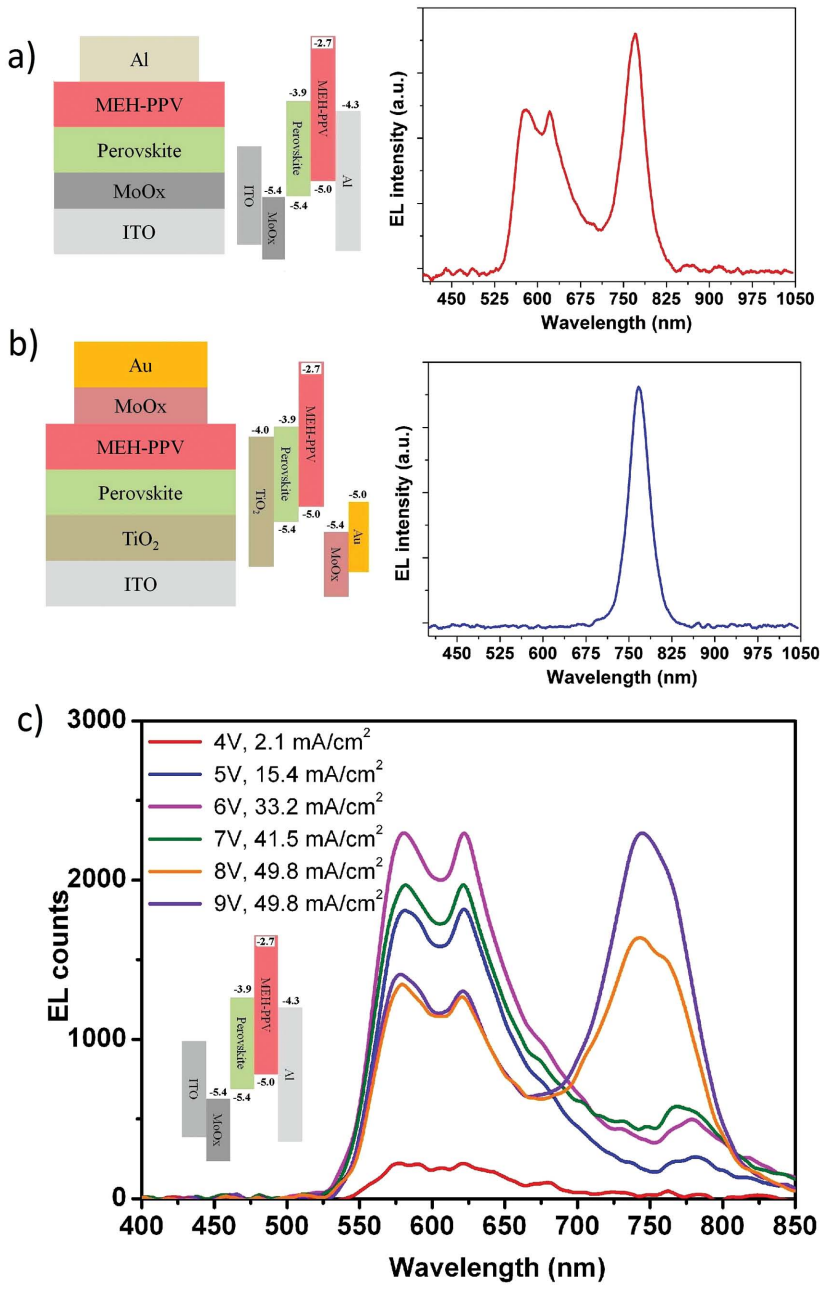

Figure 3. Device structure, flat-band energy level diagram, and electroluminescence spectra of a) ITO/MoO_x–6 nm/perovskite/MEH–PPV/Al devices and b) ITO/TiO_2/perovskite/MEH–PPV/MoO_x–10 nm/Au devices. The EL spectrum of the structure in (a) shows emission from the perovskite layer and the MEH–PPV layer while the EL spectrum of the structure in (b) shows emission from the perovskite layer only. c) Electroluminescence spectra of a standard (ITO/MoO_x–6 nm/perovskite/MEH–PPV/Al) device at various voltage biases. The respective current densities are also shown. The emission from the perovskite layer increased with the applied bias. Inset shows the schematic of the energy level alignment of the device.

difficult to apply in a sandwiched structures.[36] In our device, at lower bias, we consider that the recombination zone is confined within the MEH–PPV layer due to the accumulation of electrons next to the Al cathode. At higher voltage bias the recombination zone shifts toward the anode, i.e., from MEH–PPV layer toward the perovskite layer which results in increasing the emission from perovskite layer. This experimental observation could provide a platform for future investigation of electron–hole recombination dynamics in perovskite materials and near the organic–inorganic heterointerface of multilayer optoelectronic devices.

In summary, the 3D inorganic–organic perovskite materials have low Urbach energy. PV devices made using such perovskite material yielded efficient electroluminescence analogous to LED's, when the electron and hole currents were balanced inside the perovskite material. In addition to infrared emission from a single perovskite layer, simultaneous visible–infra-red electroluminescence was demonstrated from perovskite-conjugated polymer PV diodes, with a control of the recombination region between the perovskite layer and the luminescent hole transport polymer layer. This work provides a powerful method to study the electroluminescent recombination zone near the perovskite polymer hetero-interface alongwith studying the charge carrier recombination mechanism inside OPVs and LEDs. Moreover, the prospect of optimizing the optical band gap of perovskite material,[29,31,33,37,38] and availability of diverse variety of light emitting polymers, provides a promising future to build tailor-made efficient hybrid LEDs.

Experimental Section

Materials: MEH–PPV (M_n = 185 000) polymer was received from Cambridge Display Technology (CDT) and was used as received. Synthesis of methylammonium iodide (CH_3NH_3I) involves the following: 100 mL of absolute ethanol was used to dilute 24 mL of methylamine solution (33% in ethanol) in a 250 mL round bottom flask, followed by addition of 10 mL aqueous solution of hydriodic acid (57 wt%) under constant stirring. After 1 h of reaction time at room temperature, a rotary evaporator was used to remove the solvents from the reaction mixture. The white solid residual was then washed using dry diethyl ether and recrystallized from ethanol to get methylammonium bromide crystals (CH_3NH_3I). CH_3NH_3I and lead Chloride ($PbCl_2$ – Sigma–Aldrich 99.999% pure) are mixed in 3:1 molar ratios in *N*,*N*-Dimethylformamide (DMF) to get a 40 wt% solution of $CH_3NH_3PbI_{3-x}Cl_x$ perovskite precursor mixture.

Device Fabrication: ITO glass substrates were cleaned by sonicating it in acetone and isopropanol for 15 min successively, followed by treatment with oxygen plasma for 10 min. For making ITO/TiO_2/Perovskite/Spiro-OMeTAD/MoO_x/Au diode, 30 nm TiO_2 was deposited on the cleaned ITO substrate followed by annealing up to 500 °C.[25] The perovskite precursor solution was spin coated onto the TiO_2 layer at 2500 rpm for 60 s, and annealed at 100 °C for 90 min. The thickness of the perovskite film obtained was 350 nm. A 5% solution of spiro-OMeTAD as per Lee et al.[18] was spin coated onto the perovskite layer and the thickness of the spiro-OMeTAD layer obtained was about

150 nm. Thereafter, MoO_x (10 nm) and Au (150 nm) were successively deposited by vacuum thermal evaporation method using 8-pixel mask. The active area of the device was 6 mm^2. The devices were encapsulated and legged before testing. To make ITO/TiO_2/perovskite/MEH–PPV/MoO_x/Au hybrid device, the spiro-OMeTAD layer was replaced by 150 nm layer of MEH–PPV polymer. To make ITO/MoO_x/perovskite/MEH–PPV/Al hybrid device, 6 nm of MoO_x was deposited by vacuum thermal evaporation method on cleaned ITO substrate. The perovskite and MEH–PPV layers were deposited as described above. Thereafter, a 150 nm layer of aluminum was deposited by vacuum evaporation followed by encapsulation and legging.

LED Measurement: Current–voltage (*I–V*) characteristics were measured using a Keithley 2400 Source Measure Unit. The photon flux emitted during the scan was measured using a calibrated silicon photodetector and the external quantum efficiency (*EQE*) was calculated assuming a Lambertian emission profile. The electroluminescence spectra were measured using an optical fiber connected to a calibrated Ocean Optics USB 2000+ spectrometer.

PV Measurement: Current–voltage (*I–S–V*) characteristics were measured under 100 mW cm^{-2} equivalent AM 1.5 G conditions using an ABET Sun2000 solar simulator calibrated to a silicon reference cell, and corrected for spectral mismatch. The dark and the light *I–V* characteristics were measured using a Keithley 237 SMU.

Absorption Measurement: Photothermal deflection spectroscopy (PDS) technique was used for the absorption measurements. Films spun on quartz substrates were used for the measurements. PDS is a highly sensitive scatter free surface averaged absorption measurement technique capable of measuring absorbances down to 10^{-5}. A detailed description about the PDS setup can be found in Kronemeijer et al.[39]

Supporting Information

Supporting Information is available from the Wiley Online Library or from the author.

Acknowledgements

A.S. and A.K. contributed equally to this work. We gratefully acknowledge funding from the Engineering and Physical Sciences Research Council (EPSRC). A.K. acknowledges NRF-Singapore for a scholarship. A.S. conceptualized, fabricated, and measured the perovskite PV/LED diodes, and A.K. conceptualized and fabricated the perovskite-polymer PV/LED diodes. A.S. also fabricated and measured the perovskite-polymer PV/LED diodes. A.S. thanks Karl C. Goedel and Dr. Felix Deschler for the useful discussions.

Received: January 7, 2015
Published online: February 19, 2015

[1] M. Liu, M. B. Johnston, H. J. Snaith, *Nature* **2013**, *501*, 395.
[2] J. Burschka, N. Pellet, S.-J. Moon, R. Humphry-Baker, P. Gao, M. K. Nazeeruddin, M. Gratzel, *Nature* **2013**, *499*, 316.
[3] H. J. Snaith, *J. Phys. Chem. Lett.* **2013**, *4*, 3623.
[4] M. A. Green, A. Ho-Baillie, H. J. Snaith, *Nat. Photonics* **2014**, *8*, 506.
[5] H. Zhou, Q. Chen, G. Li, S. Luo, T. Song, H.-S. Duan, Z. Hong, J. You, Y. Liu, Y. Yang, *Science* **2014**, *345*, 542.
[6] National Renewable Energy Laboratory, Efficiency chart, http://www.nrel.gov/ncpv/images/efficiency_chart.jpg, Accessed: February 2015.
[7] Z.-K. Tan, R. S. Moghaddam, M. L. Lai, P. Docampo, R. Higler, F. Deschler, M. Price, A. Sadhanala, L. M. Pazos, D. Credgington, F. Hanusch, T. Bein, H. J. Snaith, R. H. Friend, *Nat. Nanotechnol.* **2014**, *9*, 687.
[8] K. Wojciechowski, S. D. Stranks, A. Abate, G. Sadoughi, A. Sadhanala, N. Kopidakis, G. Rumbles, C.-Z. Li, R. H. Friend, A. K. -Y. Jen, H. J. Snaith, *ACS Nano* **2014**, *8*, 12701.
[9] F. Deschler, M. Price, S. Pathak, L. E. Klintberg, D.-D. Jarausch, R. Higler, S. Hüttner, T. Leijtens, S. D. Stranks, H. J. Snaith, M. Atatüre, R. T. Phillips, R. H. Friend, *J. Phys. Chem. Lett.* **2014**, *5*, 1421.
[10] K. Chondroudis, D. B. Mitzi, *Chem. Mater.* **1999**, *11*, 3028.
[11] M. Era, S. Morimoto, T. Tsutsui, S. Saito, *Appl. Phys. Lett.* **1994**, *65*, 676.
[12] K. D. Karlin, Ed., *Progress in Inorganic Chemistry*, John Wiley & Sons, Inc., Hoboken, NJ, USA **1999**.
[13] K. Vandewal, K. Tvingstedt, A. Gadisa, O. Inganäs, J. V Manca, *Nat. Mater.* **2009**, *8*, 904.
[14] A. Kumar, G. Lakhwani, E. Elmalem, W. T. S. Huck, A. Rao, N. C. Greenham, R. H. Friend, *Energy Environ. Sci.* **2014**, *7*, 2227.
[15] S. Colella, E. Mosconi, P. Fedeli, A. Listorti, F. Gazza, F. Orlandi, P. Ferro, T. Besagni, A. Rizzo, G. Calestani, G. Gigli, F. De Angelis, R. Mosca, *Chem. Mater.* **2013**, *25*, 4613.
[16] M. Grätzel, *Nat. Mater.* **2014**, *13*, 838.
[17] H.-S. Kim, C.-R. Lee, J.-H. Im, K.-B. Lee, T. Moehl, A. Marchioro, S.-J. Moon, R. Humphry-Baker, J.-H. Yum, J. E. Moser, M. Grätzel, N.-G. Park, *Sci. Rep.* **2012**, *2*, 591.
[18] M. M. Lee, J. Teuscher, T. Miyasaka, T. N. Murakami, H. J. Snaith, *Science* **2012**, *338*, 643.
[19] L. P. Lu, D. Kabra, R. H. Friend, *Adv. Funct. Mater.* **2012**, *22*, 4165.
[20] L.-P. Lu, D. Kabra, K. Johnson, R. H. Friend, *Adv. Funct. Mater.* **2012**, *22*, 144.
[21] G. Li, C.-W. Chu, V. Shrotriya, J. Huang, Y. Yang, *Appl. Phys. Lett.* **2006**, *88*, 253503.
[22] Z. He, C. Zhong, S. Su, M. Xu, H. Wu, Y. Cao, *Nat. Photonics* **2012**, *6*, 593.
[23] V. I. Adamovich, S. R. Cordero, P. I. Djurovich, A. Tamayo, M. E. Thompson, B. W. D'Andrade, S. R. Forrest, *Org. Electron.* **2003**, *4*, 77.
[24] S. Reineke, F. Lindner, G. Schwartz, N. Seidler, K. Walzer, B. Lüssem, K. Leo, *Nature* **2009**, *459*, 234.
[25] J. M. Ball, M. M. Lee, A. Hey, H. J. Snaith, *Energy Environ. Sci.* **2013**, *6*, 1739.
[26] Y. Sun, C. J. Takacs, S. R. Cowan, J. H. Seo, X. Gong, A. Roy, A. J. Heeger, *Adv. Mater.* **2011**, *23*, 2226.
[27] S. De Wolf, J. Holovsky, S.-J. Moon, P. Löper, B. Niesen, M. Ledinsky, F.-J. Haug, J.-H. Yum, C. Ballif, *J. Phys. Chem. Lett.* **2014**, *5*, 1035.
[28] O. D. Miller, E. Yablonovitch, S. R. Kurtz, *IEEE J. Photovoltaics* **2012**, *2*, 303.
[29] A. Sadhanala, F. Deschler, T. H. Thomas, S. E. Dutton, K. C. Goedel, F. C. Hanusch, M. L. Lai, U. Steiner, T. Bein, P. Docampo, D. Cahen, R. H. Friend, *J. Phys. Chem. Lett.* **2014**, *5*, 2501.
[30] D. Cheyns, B. P. Rand, P. Heremans, *Appl. Phys. Lett.* **2010**, *97*, 033301.
[31] I. Grinberg, D. V. West, M. Torres, G. Gou, D. M. Stein, L. Wu, G. Chen, E. M. Gallo, A. R. Akbashev, P. K. Davies, J. E. Spanier, A. M. Rappe, *Nature* **2013**, *503*, 509.
[32] G. Xing, N. Mathews, S. S. Lim, N. Yantara, X. Liu, D. Sabba, M. Grätzel, S. Mhaisalkar, T. C. Sum, *Nat. Mater.* **2014**, *13*, 476.
[33] J. H. Noh, S. H. Im, J. H. Heo, T. N. Mandal, S. Il Seok, *Nano Lett.* **2013**, *13*, 1764.
[34] D. Liu, T. L. Kelly, *Nat. Photonics* **2013**, *8*, 133.
[35] J. C. de Mello, H. F. Wittmann, R. H. Friend, *Adv. Mater.* **1997**, *9*, 230.
[36] J. Zaumseil, R. H. Friend, H. Sirringhaus, *Nat. Mater.* **2006**, *5*, 69.
[37] G. E. Eperon, S. D. Stranks, C. Menelaou, M. B. Johnston, L. M. Herz, H. J. Snaith, *Energy Environ. Sci.* **2014**, *7*, 982.
[38] F. Hao, C. C. Stoumpos, D. H. Cao, R. P. H. Chang, M. G. Kanatzidis, *Nat. Photonics* **2014**, *8*, 489.
[39] A. J. Kronemeijer, V. Pecunia, D. Venkateshvaran, M. Nikolka, A. Sadhanala, J. Moriarty, M. Szumilo, H. Sirringhaus, *Adv. Mater.* **2014**, *26*, 728.

